Highly Controllable Surface Plasmon Resonance Property by Heights of Ordered Nanoparticle Arrays Fabricated *via* a Nonlithographic Route

Zhibing Zhan, Rui Xu, Yan Mi, Huaping Zhao, and Yong Lei*

Institute of Physics & Institute of Micro- and Nanotechnologies (ZIK MacroNano), Ilmenau University of Technology, 98693 Ilmenau, Germany

ABSTRACT Perfectly ordered nanoparticle arrays are fabricated on large-area substrates (>cm^2) *via* a cost-effective nonlithographic route. Different surface plasmon resonance (SPR) modes focus consequently on their own positions due to the identical shape and uniform size and distance of these plasmonic metallic nanoparticles (Ag and Au). On the basis of this and FDTD (finite-difference time-domain) simulation, this work reveals the variation of all SPR parameters (position, intensity, width, and mode) with nanoparticle heights, which demonstrates that the effect of heights are different in various stages. On increasing the heights, the major dipole SPR mode precisely blue-shifts from the near-infrared to the visible region with intensity strengthening, a peak narrowing effect, and multipole modes excitation in the UV—vis range. The intensity of multipole modes can be manipulated to be equal to or even greater than the major dipole SPR mode. After coating conformal TiO_2 shells on these nanoparticle arrays by atomic layer deposition, the strengthening of the SPR modes with increasing the heights results in the multiplying of the photocurrent (from ~2.5 to a maximum 90 μA cm^{-2}) in this plasmonic-metal—semiconductor-incorporated system. This simple but effective adjustment for all SPR parameters provides guidance for the future design of plasmonic metallic nanostructures, which is significant for SPR applications.

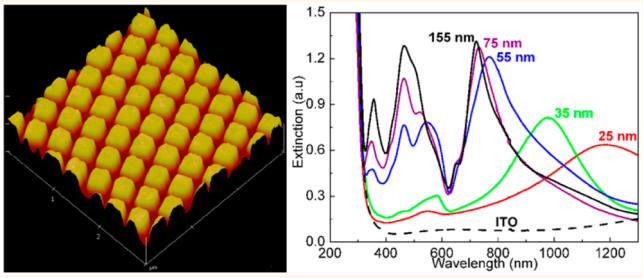

KEYWORDS: surface plasmon resonance · ordered nanoparticle arrays · nanoparticle heights · plasmonic parameters · nonlithographic route

The rapid development of surface plasmon resonance (SPR), the collective oscillation of conduction electrons across nanostructures induced by incident light, has received significant attention, due to its important applications in many fields.[1−7] In solar energy conversions, plasmonic devices offer a new opportunity to promote the efficiency by extending light absorption, increasing light scattering, and directly exciting electron−hole pairs (hot electrons).[2,3,8] As one of the most powerful probing tools in ultrasensitive analysis, surface-enhanced Raman spectroscopy (SERS) depends on the highly intense localized electromagnetic fields (also known as "hot spots") produced by the process of SPR.[4,9−11] It has been confirmed that SPR parameters (such as position, intensity, and modes) play crucial roles in plasmonic applications.[8,12,13] For example, optimizing the position and intensity of SPR is very important to improve the efficiency in solar energy conversions and upgrade the detection sensitivity of SERS.[8,12] Recently, the higher order multipole (*e.g.*, quadrupole and octupole) SPR modes caused by the phase retardation of the electromagnetic field applied inside the nanostructures have gained much attention due to potential applications in biosensing, fluorescence, nanolasers, and nonlinear nanophotonics.[14−18] Generally, these factors of SPR property are very sensitive to the parameters of plasmonic metallic nanoparticles (mainly Ag and Au) including size, shape, morphology, distribution, and surrounding environment.[19−21] As a simple, effective, and most widely used method, chemical synthesis has been used to prepare various kinds of plasmonic metallic nanostructures, such as nanospheres, nanocubes, nanowires, and nanorods.[10,11] However, with this approach it is difficult to control the distance and ordering of

* Address correspondence to yong.lei@tu-ilmenau.de.

Received for review February 24, 2015 and accepted March 26, 2015.

Published online March 26, 2015
10.1021/acsnano.5b01226

nanostructures, and it is hard to provide a perfect research model system for some aspects of the SPR effect, such as the investigation of multipole SPR modes, because multipole modes are much more sensitive to the uniformity, distribution, and ordering of nanostructures than the dipole SPR mode.[21−24] By far, it is the lithographic method that can precisely control the dimensions, interparticle spacing, and ordering of nanoparticles on substrates, such as electron beam lithography, focused ion beam lithography, and nanoimprint lithography.[25−27] However, highly specialized lithographic facilities are complex and expensive,[11] and tedious preparation and implementation steps (lithography and lift-off) require accuracy and time consumption, which restrict its application in the SPR field.[28,29] In view of this, fully controlling the SPR properties by simple techniques that allow high throughput, large pattern area, and low equipment costs are significant for the study and application of the SPR effect.[6,26]

Recently, we presented a nonlithographic route by combining the nanoimprint method with the ultrathin alumina membrane (UTAM) technique to fabricate nanoparticle arrays with perfect ordering, identical shape, and uniform size on large-scale substrates.[23] Based on this route and finite-difference time-domain (FDTD) simulation, this work exhibits a variation of all SPR parameters (position, intensity, width, and mode) with the metallic nanoparticle (Ag and Au) heights. By just increasing the nanoparticle heights, the major dipole SPR peak precisely blue-shifted from the near-infrared (NIR) to the visible region with significant intensity strengthening, a peak narrowing effect, and multipole modes excitation in the UV−vis range, which is different from general research, which reported that increasing the size of nanoparticles will result in the red-shift of the SPR peak with a broadening effect attributed to multipole excitation.[1,10,11,20] It should be noted that the multipole SPR modes can be manipulated with intensity that is equal to or even greater than the major dipole mode. After coating conformal and highly uniform TiO_2 shells on these nanoparticle arrays by atomic layer deposition (ALD), our research further showed that the strengthening of SPR modes with increasing heights resulted in the multiplying of the photocurrent (from about 2.5 to a maximum 90 μA cm^{-2}) in this plasmonic-metal−semiconductor-incorporated system. The full adjustment of SPR parameters through this simple but effective way will provide guidance for future designs of plasmonic metallic nanostructures, which is significant for applications of the SPR effect, such as in solar energy conversions (photovoltaic devices, photocatalysis, and water-splitting improved by plasmonics) and SPR-based sensing and detection (*e.g.*, the adjustment of nanoparticles with suitable SPR property corresponding to commercial lasers for SERS detection, shifting SPR peaks of Au nanoparticles to the NIR region for important applications in nanomedicine).[2,30−34] The excellent manipulation for multipole SPR modes can provide a spectroscopic fingerprint for materials and is applicable in optical fields of multipolar harmonics including those pertaining to light signal routers, light manipulators, or multistep enhancers in processes such as second-harmonic generation.[18,22] In addition, this approach provides a low-cost platform for the preparation of ordered nanostructures on large substrates, due to the replication and reuse of the imprint stamps and no need for lithographic processes and clean-room facilities.

RESULTS AND DISCUSSION

As shown in Figure 1a, the reusable Ni imprinting stamps are replicated from a commercially purchased, large silicon pattern (6 in.) with perfect arrays of nanoholes in a square lattice with distance periods of 400 nm, according to the electrodeposition method reported by Lee *et al.*[35] Our brief process includes the imprinting and anodization of the Al foil, transferring of the UTAM, deposition of materials, and removal of the UTAM, as shown in Figure 1b to h. The imprint process generates an array of highly ordered indentations on the surface of the Al foil (Figure 1c), which replicated the negative of the rounded protrusions of the Ni imprinting stamp.[36] Under suitable anodization voltage, each of the shallow indentations created by the imprinting serves as a nucleation site for the development of a pore in the early stage of anodization and results in the eventual growth of the UTAM with highly ordered pore channels (Figure 1d).[35−37] As shown from Figure 1c to h, the unique color tuning indicates the highly ordered nanostructures, because a well-ordered structure should show strong light diffraction, which can easily be examined by the naked eye.[38] Compared to many reports,[36,38] a low pressure (∼10 MP) is required in our imprinting process, because Al foil is soft and very shallow imprinted indentations (∼1.5 nm) can effectively guide the growth of the anodized nanopores,[39] which ensures the reusability of the imprinting stamps. Different from nanoimprinting lithography, the attachment of the mold to the thermoplastic is avoided due to the patterning of the Al surface,[40,41] which also benefits the reusability. All of our fabrication procedures are carried out in a routine laboratory rather than a clean-room. Detailed processes are described in the Experimental Section.

Figure 1i to k are SEM images and AFM section analysis of the Ag nanoparticle array on ITO-coated glass. In tilted (45°) SEM images of Figure 1i and j, parts of the UTAM are shown intentionally. As can be seen from these images, the transferred UTAM is a perfectly ordered arrangement of nanopores, which has no defects in a very large area. The prepared nanoparticles are uniform and monodispersed, which completely inherit the regularity of the UTAM template. Top-view

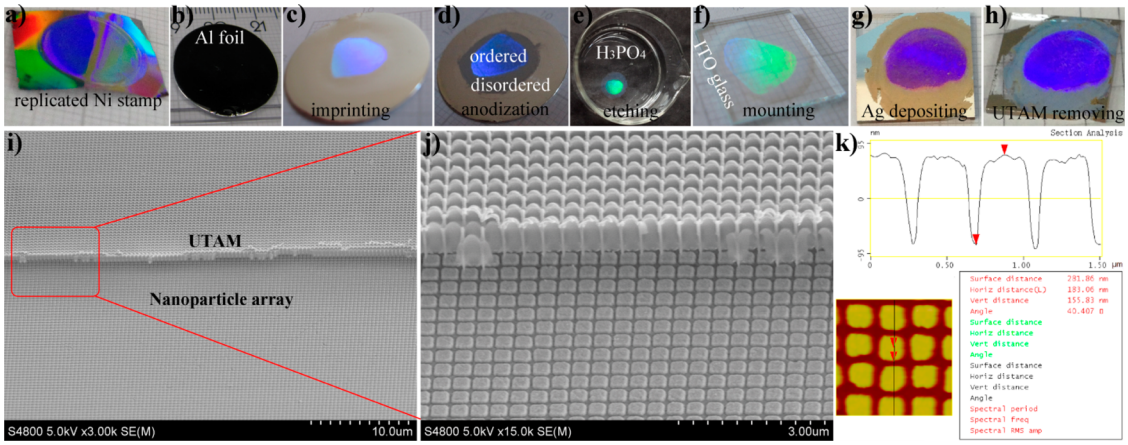

Figure 1. (a–h) Photographic outline of the fabrication of a perfectly ordered Ag nanoparticle array on an ITO-coated glass. (d) Photograph of the disordered and highly ordered parts of the UTAM. (e) Photograph showing the UTAM in a colorless H_3PO_4 solution. Large-scale (i) and high-resolution (j) SEM images (tilted 45°) and AFM section analysis (k) of the nanoparticle array deposited on an ITO-coated glass.

SEM images of the perfect UTAM and nanoparticle array with large area after totally removing the UTAM are shown in Figures S1 and S2 (Supporting Information). The cross-sectional AFM profile shown in Figure 1k further illustrates that the Ag nanoparticles kept a sharp shape even with heights as high as ~155 nm. Considering the broadening effect resulting from the size of the AFM tip, the actual shape of the nanoparticles should be sharper than that in the cross-sectional profile.[6]

SPR property is very sensitive to the structural parameters of the nanostructures, such as the dimension, shape, interparticle distance, kind, and physical and chemical surrounding environment.[5,19–21,42,43] As shown by the AFM section analyses in Figures 2 and 1k, nanoparticle arrays with different heights are prepared just by controlling the evaporation time of the metal. Except for their heights, these nanoparticles have almost identical shape, size scale, distance, and surrounding conditions, which provides a perfect research model system to study the effect of nanoparticle heights on the SPR property exclusively. These Ag nanoparticle arrays deposited on ITO-coated glasses were characterized by UV–vis–NIR extinction spectra, as shown in Figure 3a. The strong absorptions below a wavelength of 320 nm in all spectra are associated with the optical band gap of the ITO glass. Before depositing nanoparticles, the ITO glass shows a low optical absorption for wavelengths above 320 nm and does not exhibit any resonance property, as shown by the dashed curve. After depositing Ag nanoparticles with a height of ~25 nm, a clear SPR peak is detected at about 1180 nm, as shown in Figure 3a. On further increasing the heights to about 35, 55, 75, and 155 nm, the number, intensity, position, and width of the SPR peaks accelerate, strengthen, blue-shift, and narrow, respectively. In order to reveal the origins of these SPR peaks, FDTD simulations for Ag nanoparticle arrays are carried out, as shown in Figure 3b to f. The SPR peaks obtained from the calculated scattering cross section agreed well with the experimental extinction spectra, as shown in Figure 3a and b. The simulated near-field distributions around Ag nanoparticles under a series of resonance wavelengths corresponding to the calculated scattering cross section (Figure 3b) are presented in Figure 3c to f. The continuous near-field distributed at the two ends of the Ag nanoparticle represents the dipole SPR mode (Figure 3c), and the relatively separated near-field distributions indicate the multipole modes,[14,15,44] which successively appeared with quadrupole, octupole, and hexadecapole modes (Figure 3d to f). Figure 3a shows the variation of SPR with the increasing of Ag nanoparticle heights. On increasing the heights from 25 nm to 35, 55, and 75 nm, the major SPR peaks (dipole mode) of these particles display a continuous blue-shift from about 1180 nm to 980, 760, and 720 nm, respectively, with an obvious peak narrowing effect. At the same time, three types of higher order multipole SPR modes (quadrupole at ~510 nm, octupole at ~460 nm, and hexadecapole mode at ~350 nm) exhibit the process from nothing to gradually strengthening. On further increasing the height from ~75 nm to 155 nm, the peak of the dipole SPR mode shows rather weak changes in its position (just from 720 to 710 nm), intensity, and width, whereas the intensity of multipole modes strengthens significantly, and one of them is even the same as the major dipole SPR mode, as shown in Figure 3a. The extinction spectra of Au nanoparticle arrays with different heights exhibited exactly the same tendency but with a weaker blue-shift and a narrowing effect for the dipole mode, as well as one less multipole mode, as shown in Figure 4. The FDTD simulations for Au nanoparticle arrays with the same dimensions as Ag nanoparticles are shown in Figures S3 and S4. Besides the adjustment of SPR parameters by nanoparticle heights, the effects of nanoparticle dimension, spacing, and period on the SPR property have also been studied in this work.

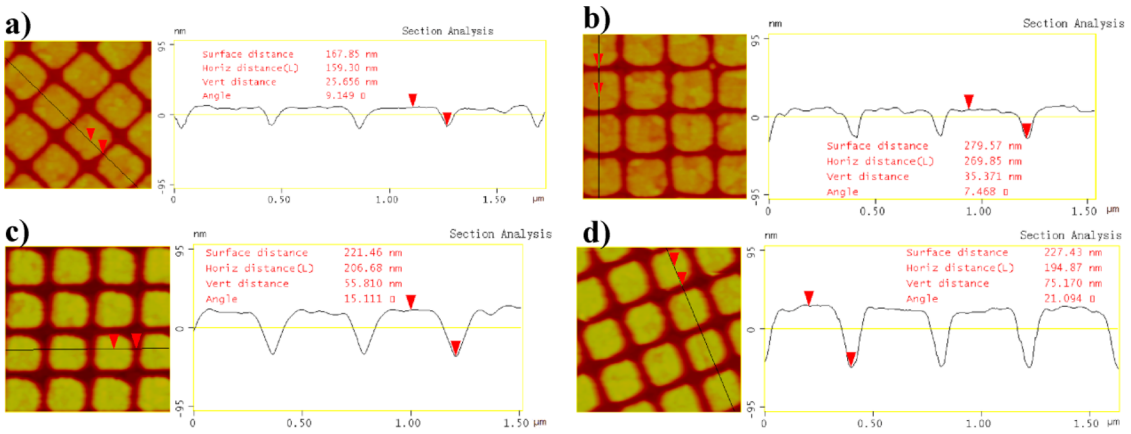

Figure 2. AFM section analyses of Ag nanoparticles with heights of about (a) 25, (b) 35, (c) 55, and (d) 75 nm.

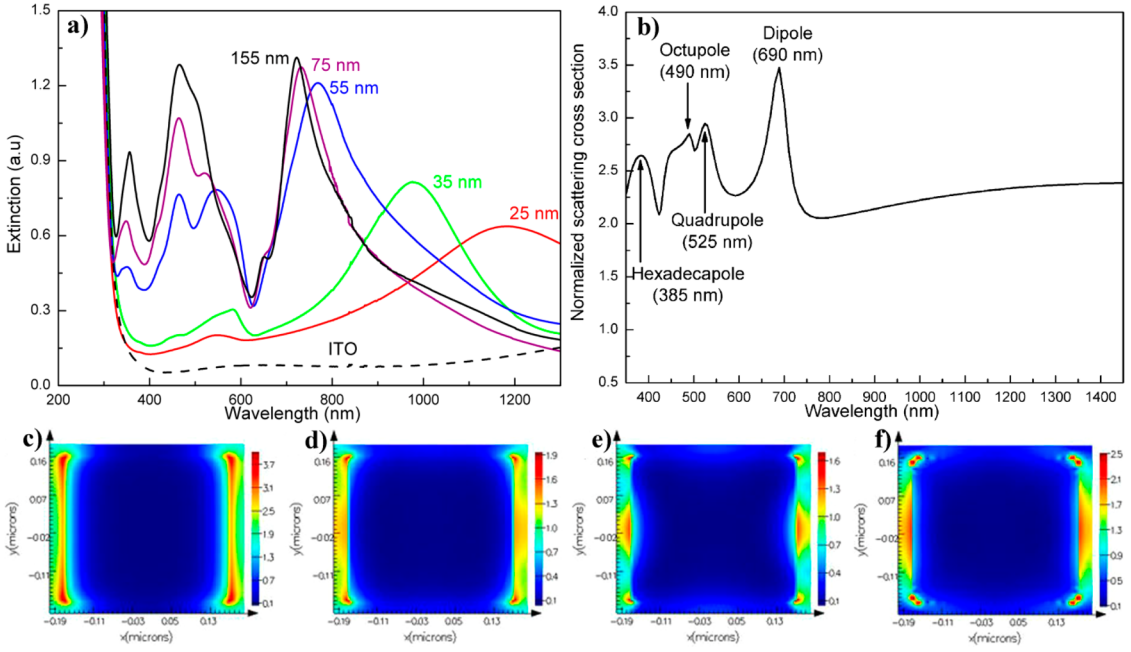

Figure 3. (a) Experimental UV−vis−NIR extinction spectra of Ag nanoparticle arrays deposited on ITO-coated glasses with heights of about 25, 35, 55, 75, and 155 nm. (b) Simulated scattering cross section for a Ag nanoparticle array with dimensions of 350 × 350 × 155 nm (length × width × height). (c−f) Calculated near-field distributions around Ag nanoparticles under a series of resonance wavelengths corresponding with those marked in (b): (c) 690, (d) 525, (e) 490, and (f) 385 nm.

As shown in Figure S5, the major dipole SPR peak can further be adjusted to about 650 and 500 nm by decreasing the Ag nanoparticle sizes to 200 and 50 nm with periods of 400 and 100 nm, respectively. Correspondingly, the number of multipole SPR modes decline to only two and one. As in many reports, the decreasing nanoparticle size resulted in the blue-shift of the major SPR mode with peak narrowing and less multipole SPR mode excitation.[10,11,20]

This systematical research clearly exhibited the variation of all SPR parameters (position, intensity, width, and mode) with nanoparticle heights and revealed that the effect of heights on these SPR parameters varied in different stages. Low heights determined the position, intensity, and width of the major SPR mode, which are almost not affected by high heights. The intensity of the multipole SPR modes strengthened with the increasing nanoparticle heights, whereas their position did not relate to the heights. Generally, increasing the size of the nanoparticles will result in a red-shift of the SPR peak with a broadening effect attributed to the multipole excitation.[1,10,11,20] However, our study confirmed that merely increasing the height will lead to a tremendous blue-shift of the major dipole SPR mode with peak narrowing and multipole mode excitation. The reasons for this blue-shift are that increasing heights strengthened the restoring force to the displaced electron gas and electromagnetic coupling among neighboring nanoparticles, which leads to a shorter resonance wavelength.[21] Furthermore, our result confirmed that the excitation of multipole SPR modes will not necessarily result in a peak broadening

effect. In fact, the width of the SPR peak is mainly involved in the uniformity of nanoparticles including size, shape, and distribution, in addition to the multipole excitation.[21,23,45] Nanoparticle arrays in our ideal model system are of identical shape with uniform dimensions and distances; different SPR modes focused consequently on their own positions, which is crucial for our revealing of all SPR information. Simply changing the nanoparticle heights exhibited an outstanding and precise adjustment for the SPR property in a very broad region, which has significance for the application of the SPR effect.[34] For example, nanoparticle arrays can be adjusted with suitable SPR peaks corresponding to commercial lasers (*e.g.*, 360, 785, and 1064 nm) for SERS application.[12,31,32] For Au nanoparticles, the shift of the SPR to the NIR region has important applications in nanomedicine, because the SPR penetration into living tissues in the NIR region is much deeper than that in the visible light and excites less background fluorescence.[31−33] The outstanding manipulation to multipole SPR modes may have important applications in optical fields of multipolar harmonics including light signal routers, light manipulators, and multistep enhancers in processes such as second-harmonic generation.[18] In addition, these higher order SPR modes can supply a spectroscopic fingerprint of the material, which can be used to detect, characterize, and assess the quality of such structures.[18] A narrow plasmon width is desirable for most plasmonic applications such as in sensors, the enhancement of nonlinear optical effects, light guiding, labeling, or tissue targeting.[46]

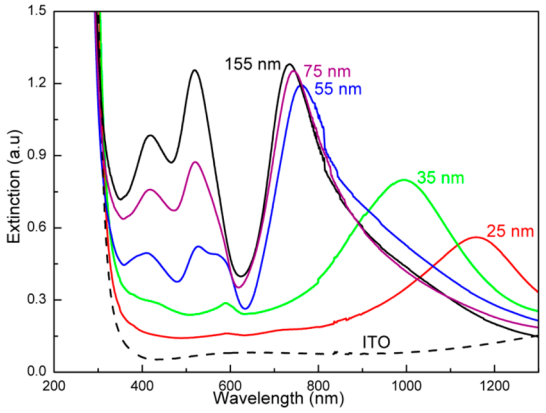

Figure 4. Experimental UV−vis−NIR extinction spectra of Au nanoparticle arrays deposited on ITO-coated glasses with heights of about 25, 35, 55, 75, and 155 nm.

To further check the effect of the SPR in the field of solar energy conversions, samples with different heights were coated with thin shells of TiO_2 by ALD to form the plasmonic-metal−semiconductor-incorporated systems and then characterized by photocurrent responses upon illumination with repeated on/off cycles of AM 1.5 light after sealing the devices by a glass tube and a layer of insulated epoxy, as shown in Figure 5a and b. As can be seen from the SEM images, the coated

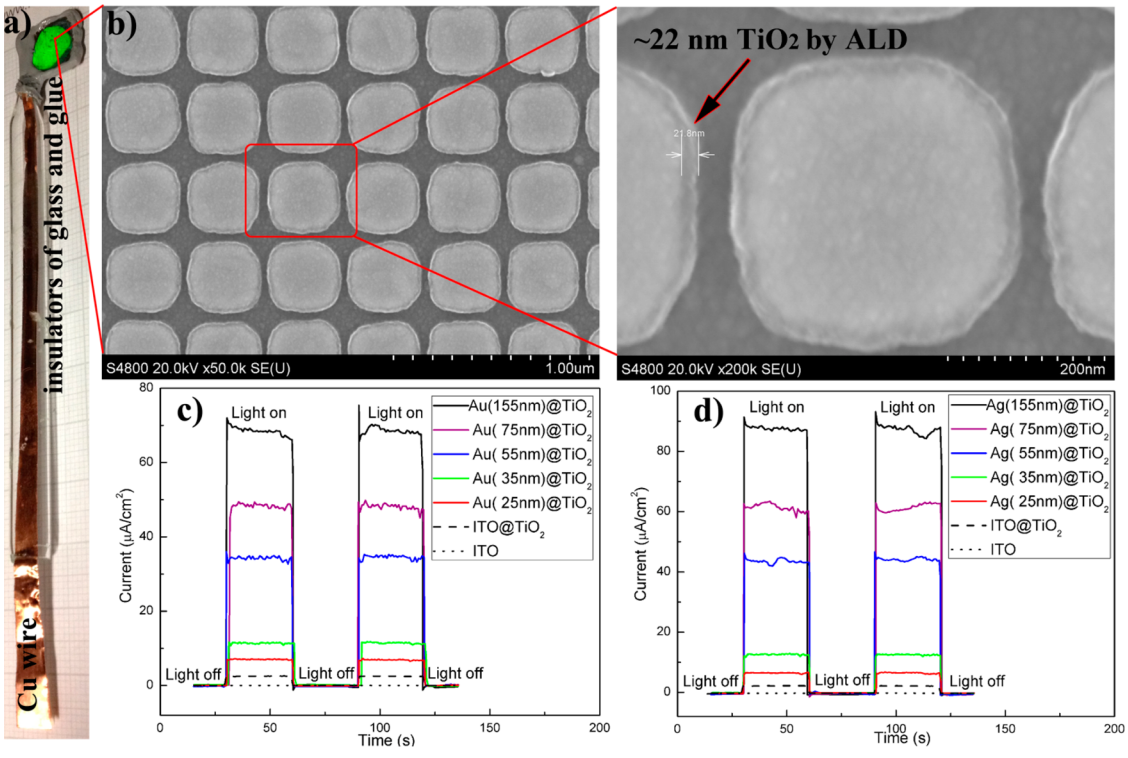

Figure 5. (a) Photograph of a device for the photocurrent responses test after coating with a thin TiO_2 shell by ALD and sealing by a glass tube and a layer of insulated epoxy; (b) top-view SEM images of Au nanoparticle arrays after coating with a thin shell of TiO_2 with a thickness of ~22 nm by ALD; and photocurrent response results of (c) Au and (d) Ag samples with repeated on/off cycles of AM 1.5 light illumination.

TiO_2 shells are compact, pinhole-free, and highly uniform, which showed their good-quality fabrication by the ALD method. The thickness of the TiO_2 shell (~22 nm) was accurately controlled by the ALD cycles (450 cycles), which also agrees with the value obtained from our other experiments. Detailed experiments are described in the Experimental Section. Photocurrents *versus* bias voltage with and without light illumination are shown in Figure S6. The results of the photocurrent responses for Au and Ag samples are shown in Figure 5c and d. For pure ITO substrates, there are no photocurrent responses, as shown by the dotted lines. After coating a thin layer of TiO_2 with the same thickness of about 22 nm on an ITO glass, a weak photocurrent response of about 2.5 μA cm^{-2} was detected under AM 1.5 illumination (dashed lines). For samples of Au nanoparticle arrays with heights of 25 and 35 nm, the photocurrent responses increased to ~7 and 12 μA cm^{-2}, as shown in Figure 5c. When the heights of Au nanoparticles reached 55, 75, and 155 nm, their photocurrent response rapidly increased to ~33, 48, and 70 μA cm^{-2}, respectively. Samples of Ag nanoparticle arrays have the same tendency with a stronger effect (Figure 5d). By increasing the height of Ag nanoparticles to 155 nm, its photocurrent can reach about 90 μA cm^{-2}, which is about 40 times more than that of pure TiO_2 samples.

The above result illustrated that the SPR effect improved the photocurrent in this incorporated system of plasmonic-metal–semiconductor nanostructures. With the increasing of nanoparticle heights, the SPR effect strengthened, which enhanced the scattering and absorption of incident light (particularly for scattering) and then resulted in the multiplying of photocurrent, especially when the major SPR mode entered the visible region.[2,11,47] Detailed mechanisms of energy transfer from these typically plasmonic metallic nanostructures (Au and Ag) to a semiconductor (TiO_2) have been intensively studied and summarized by many researchers.[2,47–49] By comparing the difference in photocurrent responses between the samples with heights of 75 and 155 nm (Figure 5c and d), we may conclude that the multipole SPR modes also have important contributions to photocarriers. This study has important applications in the fields of photovoltaic devices, photocatalysis, and water-splitting improved by plasmonics. In addition, our study experimentally confirmed that, under the same conditions, the SPR effect and its improvement in the photocurrent for Ag are stronger than those for Au, which is the reason that Ag is probably the most important material in plasmonics.[11,50]

CONCLUSION

In summary, perfectly ordered plasmonic metallic nanoparticle arrays (Ag and Au) were fabricated on large-area substrates by a low-cost nonlithographic approach. On this basis, an ideal model system was established to study the effect of nanoparticle heights on the SPR property exclusively and their improvement to photocarriers after coating with a thin TiO_2 shell by ALD. Our systematical research showed the variation of all SPR parameters (position, intensity, mode, *etc.*) with nanoparticle height and revealed that its effect varied in different stages. By just changing the heights, the SPR effect can be tuned in broad UV–vis–NIR regions, which results in the multiplying of the photocurrent. Due to this precise manipulation, this work has significance for SPR applications, such as providing guidance for the future design of plasmonic metallic nanostructures. Because of the replication and reuse of the imprinting stamps and no need for lithographic processes and clean-room facilities, the fabrication route presented here provides a cost-effective platform for the preparation of perfectly ordered nanostructures on substrates for various applications in nanotechnology.

EXPERIMENTAL SECTION

Nanoparticle Fabrication, Characterization, and Simulation. High-purity (99.99%) aluminum foil with a thickness of about 0.2 mm was degreased in acetone and annealed at 400 °C for 4 h under vacuum conditions to remove the mechanical stresses. Then it was electrochemically polished in a 1:7 solution of perchloric acid and ethanol. The reusable Ni imprinting stamp was placed on the electropolished Al foil, and pressing was carried out using an oil press under about 10 MP for 3 min. After this nanoindentation, anodization was conducted under a constant voltage of 160 V in 0.4 M H_3PO_4 at 15 °C. The anodization was performed for 8 min. For UTAMs imprinted by a SiC stamp, the imprinting pressure was about 6 MP and the anodization process was 3 min (in 0.3 M oxalic acid at 40 V). After anodization, the Al layer on the backside of the UTAM was removed in a mixture solution of $CuCl_2$ (90 wt %) and HCl (10 wt %) with a concentration of 30%. Utilizing a plastic strainer, the UTAM was transferred to a H_3PO_4 solution (5 wt %) at 30 °C to remove the barrier layer and widen the size of the pores. The durations of the barrier layer removal and pore-widening process depend on the desired sizes of the pores in the UTAMs, which are 120, 105, and 50 min for nanoparticles with sizes of about 350, 200, and 50 nm, respectively. Then the UTAM with uniform opened pores was transferred into DI water from a H_3PO_4 solution by the same plastic strainer, and the clean UTAM was mounted carefully on the substrate in DI water. Finally, the substrate mounted with a UTAM was taken out and dried, and Au (or Ag) nanoparticles were deposited into highly ordered nanopores of the UTAM by the electron beam evaporation method (Kurt J. Lesker). During the deposition process, substrates were kept in rotation at 20 rounds per minute. Then the UTAM was peeled off by Scotch tape, leaving a perfectly ordered nanoparticle array on the surface of the substrate.

The structures of the nanoparticle arrays were observed by SEM (Hitachi S4800) and AFM (Autopre CP-VEECO). Extinction spectra were collected by a UV–vis–NIR spectrophotometer (Cary 5000). A commercial FDTD simulation package (FDTD Solutions, Lumerical Solutions Inc.) was used for calculating scattering cross sections and near-field distributions of Au and Ag nanoparticle arrays.

ALD. The TiO_2 shell was deposited from the precursor of $TiCl_4$ using a Picosun SUNALETM R-150 ALD system. The chamber temperature was held at 300 °C. The $TiCl_4$ precursor and deionized H_2O were at room temperature. As the carrier gas, highly pure N_2 (99.999%) flowed at a rate of 100 sccm. The precursors were pulsed for 0.1 s each and purged with the pure N_2 flow by a 10 s pump. Clean silicon chips were coated concurrently with the samples to monitor TiO_2 film growth.

Photocurrent Responses. A glass beaker was fitted with a quartz window. The beaker was filled with 1 M KOH, which was continuously stirred with a magnetic stir bar and deaerated by the bubbling argon. After coating TiO_2 by ALD, the sample was sealed by a glass tube and a layer of insulated epoxy (Loctite EA 450 A&B) and then suspended in the beaker facing the quartz window and attached to the working electrode (EC-Lab). A Pt net counter electrode and Ag/AgCl reference electrode were used. A shutter was used to switch on/off the light with a fluence of 100 mW cm^{-2} (1 sun) derived from a xenon lamp fitted with an AM 1.5 filter (Newport).

Conflict of Interest: The authors declare no competing financial interest.

Supporting Information Available: Large-area SEM images of the perfect UTAM after Au deposition and a Au nanoparticle array after totally removing the UTAM, FDTD simulations for Au nanoparticle arrays with dimensions of 350 × 350 × 155 nm (length × width × height), UV−vis−NIR extinction spectra and corresponding SEM images of Ag nanoparticle arrays deposited on ITO-coated glasses with dimensions of 200 × 200 × 55 nm (period of 400 nm) and 50 × 50 × 55 nm (period of 100 nm), and photocurrent *versus* bias voltage of the Ag nanoparticle array after coating with a TiO_2 shell with and without AM 1.5 illumination. This material is available free of charge *via* the Internet at http://pubs.acs.org.

Acknowledgment. This work was supported by a European Research Council Grant (Three-D Surface: 240144), Federal Ministry of Education and Research in Germany (BMBF: ZIK-3DNano-Device: 03Z1MN11), and Volkswagen-Stiftung (Herstellung Funktionaler Oberflächen: I/83 984). We thank Ms. Danmei Pan from the Fujian Institute of Research on the Structure of Matter, Chinese Academy of Sciences, for the AFM measurement help; Dr. Chengliang Wang for the electron beam evaporation experiment; and Mr. Liaoyong Wen, Dr. Zhijie Wang, and Dr. Dawei Cao for help with photocurrent response experiments. The authors also thank Ms. Moumou Li, Dr. Arne Albrecht, Dr. Alexander Konkin, and Dr. Henry Romanus for technical support.

REFERENCES AND NOTES

1. Saha, K.; Agasti, S. S.; Kim, C.; Li, X. N.; Rotello, V. M. Gold Nanoparticles in Chemical and Biological Sensing. *Chem. Rev.* **2012**, *112*, 2739–2779.
2. Cushing, S. K.; Li, J. T.; Meng, F. K.; Senty, T. R.; Suri, S.; Zhi, M. J.; Li, M.; Bristow, A. D.; Wu, N. Q. Photocatalytic Activity Enhanced by Plasmonic Resonant Energy Transfer from Metal to Semiconductor. *J. Am. Chem. Soc.* **2012**, *134*, 15033–15041.
3. Mubeen, S.; Lee, J.; Singh, N.; Kraemer, S.; Stucky, G. D.; Moskovits, M. An Autonomous Photosynthetic Device in Which All Charge Carriers Derive from Surface Plasmons. *Nat. Nanotechnol.* **2013**, *8*, 247–251.
4. Della Gaspera, E.; Bersani, M.; Mattei, G.; Tich-Lam, N.; Mulvaney, P.; Martucci, A. Cooperative Effect of Au and Pt inside TiO_2 Matrix for Optical Hydrogen Detection at Room Temperature Using Surface Plasmon Spectroscopy. *Nanoscale* **2012**, *4*, 5972–5979.
5. Niu, Z.; Zhen, Y.; Gong, M.; Peng, Q.; Nordlander, P.; Li, Y. Pd Nanocrystals with Single-, Double-, and Triple-Cavities: Facile Synthesis and Tunable Plasmonic Properties. *Chem. Sci.* **2011**, *2*, 2392–2395.
6. Haynes, C. L.; Van Duyne, R. P. Nanosphere Lithography: A Versatile Nanofabrication Tool for Studies of Size-Dependent Nanoparticle Optics. *J. Phys. Chem. B* **2001**, *105*, 5599–5611.
7. Linic, S.; Christopher, P.; Ingram, D. Plasmonic-Metal Nanostructures for Efficient Conversion of Solar to Chemical Energy. *Nat. Mater.* **2011**, *10*, 911–921.
8. Zhang, Z.; Zhang, L.; Hedhili, M. N.; Zhang, H.; Wang, P. Plasmonic Gold Nanocrystals Coupled with Photonic Crystal Seamlessly on TiO_2 Nanotube Photoelectrodes for Efficient Visible Light Photoelectrochemical Water Splitting. *Nano Lett.* **2013**, *13*, 14–20.
9. Goh, M. S.; Lee, Y. H.; Pedireddy, S.; Phang, I. Y.; Tjiu, W. W.; Tan, J. M. R.; Ling, X. Y. A Chemical Route to Increase Hot Spots on Silver Nanowires for Surface-Enhanced Raman Spectroscopy Application. *Langmuir* **2012**, *28*, 14441–14449.
10. Xia, Y.; Xiong, Y.; Lim, B.; Skrabalak, S. E. Shape-Controlled Synthesis of Metal Nanocrystals: Simple Chemistry Meets Complex Physics? *Angew. Chem., Int. Ed.* **2009**, *48*, 60–103.
11. Rycenga, M.; Cobley, C. M.; Zeng, J.; Li, W.; Moran, C. H.; Zhang, Q.; Qin, D.; Xia, Y. Controlling the Synthesis and Assembly of Silver Nanostructures for Plasmonic Applications. *Chem. Rev.* **2011**, *111*, 3669–3712.
12. Orendorff, C. J.; Gearheart, L.; Jana, N. R.; Murphy, C. J. Aspect Ratio Dependence on Surface Enhanced Raman Scattering Using Silver and Gold Nanorod Substrates. *Phys. Chem. Chem. Phys.* **2006**, *8*, 165–170.
13. Gu, G. H.; Kim, J.; Kim, L.; Suh, J. S. Optimum Length of Silver Nanorods for Fabrication of Hot Spots. *J. Phys. Chem. C* **2007**, *111*, 7906–7909.
14. Yin, J.; Zang, Y.; Xu, B.; Li, S.; Kang, J.; Fang, Y.; Wu, Z.; Li, J. Multipole Plasmon Resonances in Self-Assembled Metal Hollow-Nanospheres. *Nanoscale* **2014**, *6*, 3934–3940.
15. Kumbhar, A. S.; Kinnan, M. K.; Chumanov, G. Multipole Plasmon Resonances of Submicron Silver Particles. *J. Am. Chem. Soc.* **2005**, *127*, 12444–12445.
16. Lal, S.; Link, S.; Halas, N. J. Nano-Optics from Sensing to Waveguiding. *Nat. Photonics* **2007**, *1*, 641–648.
17. Khlebtsov, B. N.; Khlebtsov, N. G. Multipole Plasmons in Metal Nanorods: Scaling Properties and Dependence on Particle Size, Shape, Orientation, and Dielectric Environment. *J. Phys. Chem. C* **2007**, *111*, 11516–11527.
18. Payne, E. K.; Shuford, K. L.; Park, S.; Schatz, G. C.; Mirkin, C. A. Multipole Plasmon Resonances in Gold Nanorods. *J. Phys. Chem. B* **2006**, *110*, 2150–2154.
19. Mulvaney, P.; Perez-Juste, J.; Giersig, M.; Liz-Marzan, L. M.; Pecharroman, C. Drastic Surface Plasmon Mode Shifts in Gold Nanorods Due to Electron Charging. *Plasmonics* **2006**, *1*, 61–66.
20. Zhang, Q.; Li, W.; Moran, C.; Zeng, J.; Chen, J.; Wen, L.-P.; Xia, Y. Seed-Mediated Synthesis of Ag Nanocubes with Controllable Edge Lengths in the Range of 30−200 nm and Comparison of Their Optical Properties. *J. Am. Chem. Soc.* **2010**, *132*, 11372–11378.
21. Henson, J.; DiMaria, J.; Paiella, R. Influence of Nanoparticle Height on Plasmonic Resonance Wavelength and Electromagnetic Field Enhancement in Two-Dimensional Arrays. *J. Appl. Phys.* **2009**, *106*, 093111.
22. Gao, S.; Ueno, K.; Misawa, H. Plasmonic Antenna Effects on Photochemical Reactions. *Acc. Chem. Res.* **2011**, *44*, 251–260.
23. Zhan, Z. B.; Lei, Y. Sub-100-nm Nanoparticle Arrays with Perfect Ordering and Tunable and Uniform Dimensions Fabricated by Combining Nanoimprinting with Ultrathin Alumina Membrane Technique. *ACS Nano* **2014**, *8*, 3862–3868.
24. Fan, J. A.; Wu, C.; Bao, K.; Bao, J.; Bardhan, R.; Halas, N. J.; Manoharan, V. N.; Nordlander, P.; Shvets, G.; Capasso, F. Self-Assembled Plasmonic Nanoparticle Clusters. *Science* **2010**, *328*, 1135–1138.
25. Guo, L. J. Nanoimprint Lithography: Methods and Material Requirements. *Adv. Mater.* **2007**, *19*, 495–513.
26. Gates, B. D.; Xu, Q. B.; Stewart, M.; Ryan, D.; Willson, C. G.; Whitesides, G. M. New Approaches to Nanofabrication: Molding, Printing, and Other Techniques. *Chem. Rev.* **2005**, *105*, 1171–1196.
27. Kramer, S.; Fuierer, R. R.; Gorman, C. B. Scanning Probe Lithography Using Self-Assembled Monolayers. *Chem. Rev.* **2003**, *103*, 4367–4418.

28. Timmermans, M. Y.; Grigoras, K.; Nasibulin, A. G.; Hurskainen, V.; Franssila, S.; Ermolov, V.; Kauppinen, E. I. Lithography-Free Fabrication of Carbon Nanotube Network Transistors. *Nanotechnology* **2011**, *22*, 065303.
29. Lei, Y.; Cai, W.; Wilde, G. Highly Ordered Nanostructures with Tunable Size, Shape and Properties: A New Way to Surface Nano-Patterning Using Ultra-Thin Alumina Masks. *Prog. Mater. Sci.* **2007**, *52*, 465–539.
30. Liu, H.; Sun, Y.; Jin, Z.; Yang, L.; Liu, J. Capillarity-Constructed Reversible Hot Spots for Molecular Ttrapping Inside Silver Nanorod Arrays Light up Ultrahigh SERS Enhancement. *Chem. Sci.* **2013**, *4*, 3490–3496.
31. Murphy, C. J.; Gole, A. M.; Hunyadi, S. E.; Stone, J. W.; Sisco, P. N.; Alkilany, A.; Kinard, B. E.; Hankins, P. Chemical Sensing and Imaging with Metallic Nanorods. *Chem. Commun.* **2008**, 544–557.
32. Boisselier, E.; Astruc, D. Gold Nanoparticles in Nanomedicine: Preparations, Imaging, Diagnostics, Therapies and Toxicity. *Chem. Soc. Rev.* **2009**, *38*, 1759–1782.
33. Sun, Y. G.; Xia, Y. N. Mechanistic Study on the Replacement Reaction between Silver Nanostructures and Chloroauric Acid in Aqueous Medium. *J. Am. Chem. Soc.* **2004**, *126*, 3892–3901.
34. Liu, Z. W.; Hou, W. B.; Pavaskar, P.; Aykol, M.; Cronin, S. B. Plasmon Resonant Enhancement of Photocatalytic Water Splitting under Visible Illumination. *Nano Lett.* **2011**, *11*, 1111–1116.
35. Lee, W.; Ji, R.; Ross, C. A.; Gosele, U.; Nielsch, K. Wafer-Scale Ni Imprint Stamps for Porous Alumina Membranes Based on Interference Lithography. *Small* **2006**, *2*, 978–982.
36. Masuda, H.; Yamada, H.; Satoh, M.; Asoh, H.; Nakao, M.; Tamamura, T. Highly Ordered Nanochannel-Array Architecture in Anodic Alumina. *Appl. Phys. Lett.* **1997**, *71*, 2770–2772.
37. Robinson, A. P.; Burnell, G.; Hu, M. Z.; MacManus-Driscoll, J. L. Controlled, Perfect Ordering in Ultrathin Anodic Aluminum Oxide Templates on Silicon. *Appl. Phys. Lett.* **2007**, *91*, 143123.
38. Kustandi, T. S.; Loh, W. W.; Gao, H.; Low, H. Y. Wafer-Scale Near-Perfect Ordered Porous Alumina on Substrates by Step and Flash Imprint Lithography. *ACS Nano* **2010**, *4*, 2561–2568.
39. Chen, B.; Lu, K.; Tian, Z. Understanding Focused Ion Beam Guided Anodic Alumina Nanopore Development. *Electrochim. Acta* **2011**, *56*, 9802–9807.
40. Dumond, J. J.; Low, H. Y. Recent Developments and Design Challenges in Continuous Roller Micro- and Nanoimprinting. *J. Vac. Sci. Technol. B* **2012**, *30*, 010801.
41. Chou, S. Y.; Krauss, P. R.; Renstrom, P. J. Imprint Lithography with 25-Nanometer Resolution. *Science* **1996**, *272*, 85–87.
42. Liang, H.; Rossouw, D.; Zhao, H.; Cushing, S. K.; Shi, H.; Korinek, A.; Xu, H.; Rosei, F.; Wang, W.; Wu, N.; *et al.* Asymmetric Silver "Nanocarrot" Structures: Solution Synthesis and Their Asymmetric Plasmonic Resonances. *J. Am. Chem. Soc.* **2013**, *135*, 9616–9619.
43. Marimuthu, A.; Zhang, J. W.; Linic, S. Tuning Selectivity in Propylene Epoxidation by Plasmon Mediated Photo-Switching of Cu Oxidation State. *Science* **2013**, *339*, 1590–1593.
44. Wu, Y. P.; Nordlander, P. Finite-Difference Time-Domain Modeling of the Optical Properties of Nanoparticles Near Dielectric Substrates. *J. Phys. Chem. C* **2010**, *114*, 7302–7307.
45. Haiss, W.; Thanh, N. T. K.; Aveyard, J.; Fernig, D. G. Determination of Size and Concentration of Gold Nanoparticles from UV-Vis Spectra. *Anal. Chem.* **2007**, *79*, 4215–4221.
46. Becker, J.; Zins, I.; Jakab, A.; Khalavka, Y.; Schubert, O.; Soennichsen, C. Plasmonic Focusing Reduces Ensemble Linewidth of Silver-Coated Gold Nanorods. *Nano Lett.* **2008**, *8*, 1719–1723.
47. Ingram, D. B.; Linic, S. Water Splitting on Composite Plasmonic-Metal/Semiconductor Photoelectrodes: Evidence for Selective Plasmon-Induced Formation of Charge Carriers Near the Semiconductor Surface. *J. Am. Chem. Soc.* **2011**, *133*, 5202–5205.
48. Li, J. T.; Cushing, S. K.; Bright, J.; Meng, F. K.; Senty, T. R.; Zheng, P.; Bristow, A. D.; Wu, N. Q. Ag@Cu_2O Core-Shell Nanoparticles as Visible-Light Plasmonic Photocatalysts. *ACS Catal.* **2013**, *3*, 47–51.
49. Furube, A.; Du, L.; Hara, K.; Katoh, R.; Tachiya, M. Ultrafast Plasmon-Induced Electron Transfer from Gold Nanodots into TiO_2 Nanoparticles. *J. Am. Chem. Soc.* **2007**, *129*, 14852–14853.
50. Gao, C. B.; Lu, Z. D.; Liu, Y.; Zhang, Q.; Chi, M. F.; Cheng, Q.; Yin, Y. D. Highly Stable Silver Nanoplates for Surface Plasmon Resonance Biosensing. *Angew. Chem., Int. Ed.* **2012**, *51*, 5629–5633.